Opto-Mechanical Analysis of Segmented/Adaptive Optics

Victor Genberg, Gregory Michels
Sigmadyne, Inc. Rochester, NY

ABSTRACT

In an effort to get larger primary mirrors for both space and ground-based telescopes, many proposed designs are either segmented or adaptive or both. This paper discusses many practical analysis issues concerning the prediction of performance of these large mirrors. Topics include 1) correctability with and without focus control, 2) dynamic response analysis, 3) segment pointing and surface RMS.

Keywords: Opto-Mechanical Analysis, Adaptive, Segmented

1.0 SEGMENTED AND ADAPTIVE OPTICS

1.1 Segmented Optic

In an effort to create very large primary mirrors, an optic may be subdivided into several individual pieces (Fig 1-A) as in the Keck Telescope. This facilitates manufacturing and processing.

1.2 Deployable Optic

For large space-based mirrors, a segmented primary mirror may be folded into a smaller package to fit a launch vehicle. On orbit, the segments fold out (Fig 1-B) into a useable array, as in the proposed NGST.

1.3 Adaptive Optic

As optics get larger and lighter, they become more flexible. Actuators may be used to deform a mirror (Fig 1-C) to correct unwanted aberrations in the image, typically due to gravity, thermal, or atmospheric distortions.

Figure 1-A: Segmented

Figure 1-B: Deployable

Figure 1-C: Adaptive

The opto-mechanical analysis of these systems requires special tools and modeling techniques which are addressed in the following sections.

1.4 Example

Throughout this paper a simple, segmented, adaptive primary mirror (Fig 2-A) is used as an example. All 7 segments are identical lightweight, fused silica construction, each with a 3 point connection to a titanium truss-like mount (Fig 2-B). For illustration purposes, the discussion may refer to the 7 member assembly or simply to the center segment .

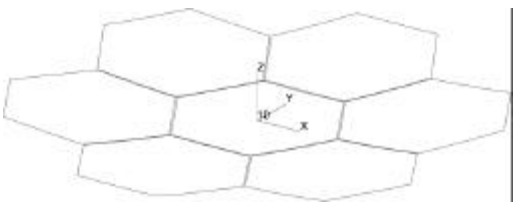

Figure 2-A: Segmented Mirror Example

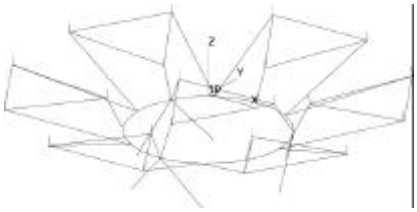

Figure 2-B: Mirror Support Structure

2.0 SURFACE DEFORMATION DESCRIPTION

2.1 Scalar Surface Deviation

When quantifying the deformation of an optical surface, it is necessary to compute a quantity we shall refer to as the *scalar surface deviation* [3]. The scalar surface deviation is computed from the optical surface geometry and the displacement vector, dX, as obtained from a finite element analysis. This scalar surface deviation physically represents the deviation of the deformed optical surface from the undeformed optical surface at each point on the optical surface. This quantity may be expressed as a deviation along the optical axis, dz*, or normal to the surface, dn*. Figure 3 shows a pictorial representation of how the scalar surface deviation is defined.

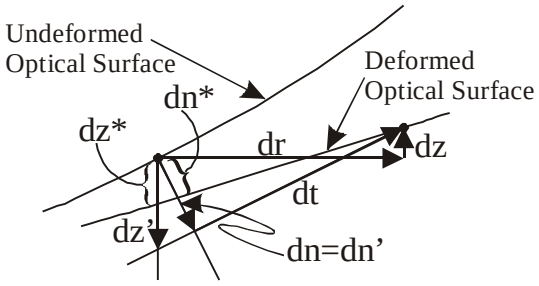

Figure 3: Surface Deformations

If the grids on an optical surface contain neither radial displacements nor azimuthal rotations, then the axial scalar surface deviation, dz*, is equal to the axial component of dX, dz. If the azimuthal rotations are absent then the normal scalar surface deviation, dn*, is equal to the normal component of dX, dn. However, if the radial displacements and/or azimuthal rotations are nonzero, then determination of the scalar surface deviations, dz* and dn*, are not as trivial. Consider the undisplaced point located at r_0, θ_0, z_0 on the conic surface given by,

$$z(r) = \frac{cr^2}{1+\sqrt{1-(1+k)c^2r^2}} \qquad 2.1\ (1)$$

with curvature c, radial location r, conic constant k, and SAG z. Suppose this point displaces dr, dz and rotates $d\theta_t$ due to rigid motions and elastic deformations of the optical surface. The exact axial and normal surface scalar deviations are referred to as dz* and dn* but are unobtainable as shown in Figure 3. However, these quantities are well approximated by the following first order Taylor series small displacement approximations:

$$dz' = dz - \left(\frac{\partial z(r_0)}{\partial r} + \left(dq_x \sin(q_0) - dq_y \cos(q_0) \right) \right) \sqrt{dx^2 + dy^2} \qquad 2.1\ (2)$$

$$dn' = dn + \left(dq_x \sin(q_0) - dq_y \cos(q_0) \right) \sqrt{dx^2 + dy^2}\,. \qquad 2.1\ (3)$$

Notice that Equations 2.1 (2) and 2.1 (3) include the effect of all of the rigid body motions of the optical surface in the calculation of the scalar surface deviation. However, these relations may be modified to compute the surface scalar deviations without the decenter rigid body motions, dc_x, dc_y, as follows:

$$dz' = dz - \left(\frac{\partial z(r_0)}{\partial r} + \left(dq_x \sin(q) - dq_y \cos(q) \right) \right) \sqrt{(dx - dc_x)^2 + (dy - dc_y)^2} \qquad 2.1\ (4)$$

$$dn' = dn + \left(dq_x \sin(q) - dq_y \cos(q) \right) \sqrt{(dx - dc_x)^2 + (dy - dc_y)^2} \qquad 2.1\ (5)$$

Equations 2.1 (4) and 2.1 (5) can be linearized by dropping the nonlinear term, $\left(dq_x \sin(q) - dq_y \cos(q) \right)$. The resulting relations become,

$$dz' = dz - \left(\frac{\partial z(r_0)}{\partial r} \right) \sqrt{(dx - dc_x)^2 + (dy - dc_y)^2} \qquad 2.1\ (6)$$

$$dn' = dn \qquad 2.1\ (7)$$

Notice that the linearized approximation to the normal surface deviation is equal to the normal surface displacement while the axial scalar surface deviation in Equation 2.1 (6) involves all of the translational displacements, dx, dy, and dz as well as the rigid body optical surface decenters.

It is important to note that the Taylor series approximation in Equation 2.1 (6) becomes less valid for decreasing r#, where r# is defined as the ratio of the optical surface diameter to its radius of curvature. However, this limitation becomes significant only for very low r#s near about 0.6.

The rotational degrees of freedom without the effect of the decenters can be approximated by a first order Taylor series similar to Equation 2.1 (4).

$$dq_t' = \left(dq_x \sin(q) - dq_y \cos(q)\right) + \left(\frac{\partial^2 z(r_0)}{\partial r^2} + \left(-\frac{\partial dq_x}{\partial r}\sin(q) + \frac{\partial dq_y}{\partial r}\cos(q)\right)\right) \times \sqrt{(dx - dc_x)^2 + (dy - dc_y)^2} \qquad 2.1\ (8)$$

which as in Equation 2.1 (6) linearizes to,

$$dq_t' = \left(dq_x \sin(q) - dq_y \cos(q)\right) + \left(\frac{\partial^2 z(r_0)}{\partial r^2}\right)\sqrt{(dx - dc_x)^2 + (dy - dc_y)^2}\,. \qquad 2.1\ (9)$$

The use of either normal or axial scalar surface deviation as discussed above is application dependent and becomes an increasingly important choice with decreasing r#. For example, if finite element results are to be formatted for import into an optical analysis code, the user should make a choice consistent with the convention used by the optical analysis software.

The necessity of computing the scalar surface deviation instead of simply using the axial displacement from the finite element analysis results can be demonstrated with an example. The following plots show a mirror with a uniform temperature increase causing an increase in the radius of curvature. The original finite element Z displacements (Fig 4-A) show the outer edge rising relative to the center (decreasing RoC), but a plot of the scalar surface deviation (Fig 4-B) shows the outer edge falls relative to the center (increasing RoC).

These two representations of the surface deformation are of opposite sign while the scalar surface deviation shows the correct flattening of the mirror. Therefore, use of the scalar surface deviation in computation of optical surface deformation is very important.

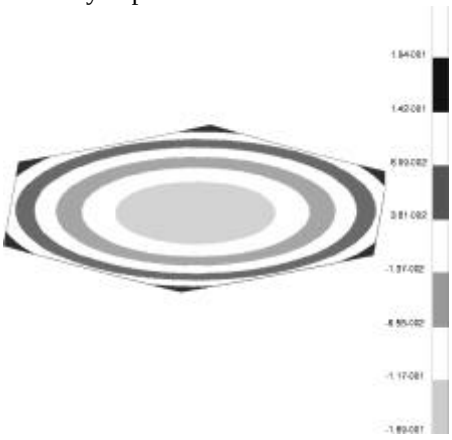

Figure 4-A: Original Z displacements (dz)

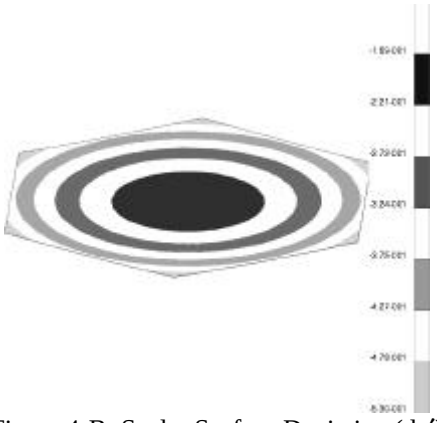

Figure 4-B: Scalar Surface Deviation (dz′)

2.2 Rigid Body Correction

FE displacements are measured from an arbitrary reference defined by the structural BC. Typically a best-fit plane (BFP) or rigid-body (R-B) motion must be removed in order for elastic distortions to be seen. Optically this is similar to pointing alignment. Rigid body motions are represented by the first 3 terms in a Zernike fit[1] of finite element results. For an optic (the center segment in the example) on a elastic mount subjected to both lateral 1g load and a uniform temperature increase, the rigid body tilt may dominate the response as shown in Table 1 and Figure 5-A. Once the rigid body motion has been subtracted, the elastic deformation can be seen in Figure 5-B (displacements in microns).

Table 1: Zernike fit to an optic subjected to 1g lateral and +55C uniform temperature

```
================================================================================
Sigmadyne, Inc.       SigFit  Version=06/28/01           10-Jul-01  15:49:45
--------------------------------------------------------------------------------
HEXAGONAL ADAPTIVE MIRROR W TITANIUM MOUNT
LOADS = +55C AND 1G -Y
--------------------------------------------------------------------------------
INPUT SURFACE: Best-Fit Zernike Polynomial Coefficients
```

Order K	N	M	Aberration	Magnitude (Waves)	Phase (Deg)	Residual RMS	Residual P-V
			Input Surface			2.7558	10.4293
1	0	0	Bias	-.34905	.0	2.7374	10.4293
2	1	1	Tilt	5.97541	90.0	.0953	.3798
3	2	0	Power (Defocus)	-.18004	.0	.0148	.0688
4	2	2	Pri Astigmatism	.04105	0.0	.0013	.0053
5	3	1	Pri Coma	.00076	90.0	.0012	.0053
6	3	3	Pri Trefoil	.00062	30.0	.0012	.0053
7	4	0	Pri Spherical	-.00019	.0	.0012	.0050
8	4	2	Sec Astigmatism	.00412	90.0	.0004	.0033
9	4	4	Pri Tetrafoil	.00149	0.0	.0003	.0015
10	5	1	Sec Coma	.00028	-90.0	.0002	.0015
11	5	3	Sec Trefoil	.00019	-30.0	.0002	.0015
12	5	5	Pri Pentafoil	.00039	18.0	.0002	.0011
13	6	0	Sec Spherical	.00000	.0	.0002	.0011
14	6	2	Ter Astigmatism	.00019	0.0	.0002	.0012
15	6	4	Sec Tetrafoil	.00009	0.0	.0002	.0012

..... truncated

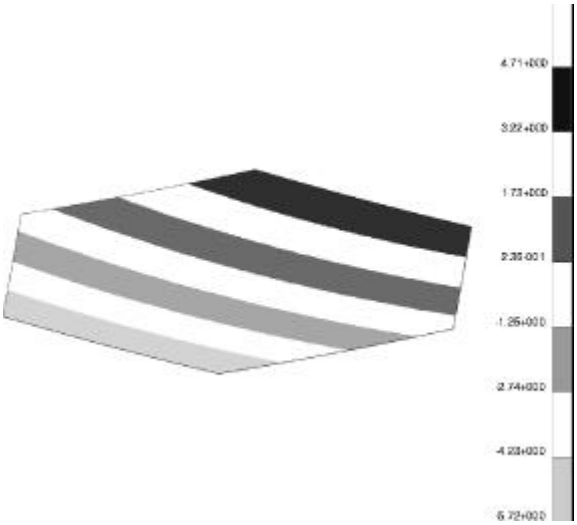

Figure 5-A: Mirror Displacement Contours
RMS=2.7 microns

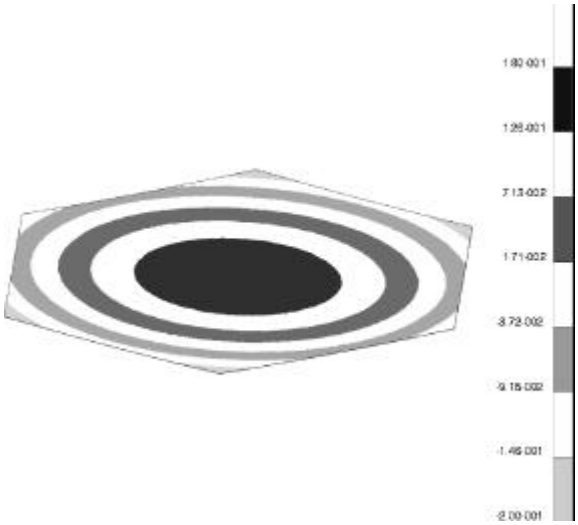

Figure 5-B: Mirror with Rigid Body Removed
RMS=0.095 microns

2.3 RoC or Power Removal

In many situations it is desired that either the best-fit radius of curvature (RoC) or the best-fit power be removed from the surface deformation description. Power shall henceforth be defined as the Z05 Born and Wolf[2] or the Z04 fringe Zernike term, $2\rho^2$-1. Example situations where power or radius of curvature change would be removed from surface deformation data include the following:

- the optical performance budget tracks radius of curvature or power changes separately from wavefront error
- an optical test is to be simulated in which the effects of bias and power are unobservable
- an optical system which images an object at infinity has capability to refocus thus removing power from a reflective surface placed at the aperture stop

When power is removed from surface in Figure 5-B, the astigmatism becomes apparent in Figure 5-C.

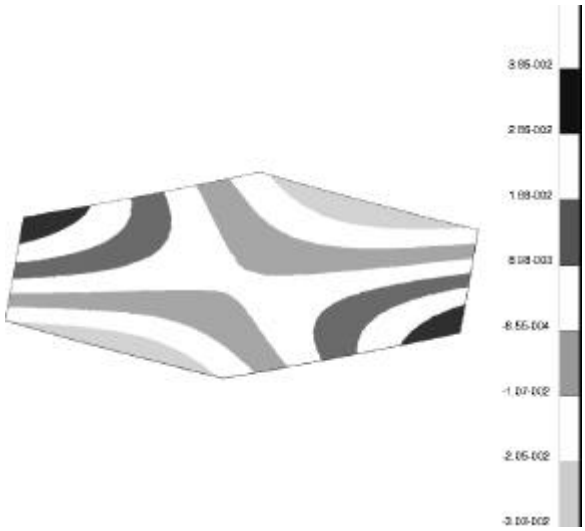

Figure 5-C: Mirror with R-B and Power Removed RMS=0.015 microns

3.0 ADAPTIVE CORRECTABILITY

3.1 Actuators

Actuators are used to displace (rigid-body) and distort an optic. Typically, the purpose is to correct pointing errors and surface aberrations due to fabrication and assembly errors, thermoelastic distortion, atmospheric disturbance or dynamic response. There are two common types of actuators in use, force (including moment) and displacement (including rotation). Their typical characteristics are as follows:

Force Actuators:	Displacement Actuators:
Apply a force or moment	Enforce a displacement or rotation
Example: voice coil	Example: piezoelectric
Have negligible stiffness	Have high stiffness
Produce global response	Produce local response

Two common design approaches for adaptive optics in the literature are:

1) Thin faceplate mirror on a dense field of displacement actuators
2) Stiffened lightweight mirror with a lower number of force actuators

Design trade issues include:

1) Degree of correctability
2) Total weight and cost: optic + actuators + reaction structure
3) Total reliability: actuator failure effect, number actuators
4) Performance: 1g test, dynamic response, thermoelastic response

From a mathematical point of view, there is no difference between force and displacement actuators. In fact, for the same mirror and placement of actuators, the correctability of perfect force and perfect displacement are the same. The difference comes from second order effects such as bending stiffness of displacement actuators or interaction with the reaction structure. In Figure 6, the actuators are "perfect" (i.e., pure normal force or pure normal displacement). The results of actuator correction as given in Table 2 show that the residual surface RMS is the same for both actuator types.

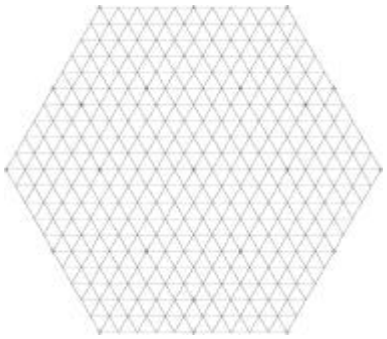

Fig 6-A: Segment Model with 22 Actuators

Fig 6-B: Single Displacement Influece Function

Fig 6-C: Single Force Actuator Influence Function

Fig 6-D: Corrected 1g Surface for Either Force/Displacement

Table 2: Correctability as Calculated by SigFit for Deformation Under 1g

Displacement Actuators

Load	Surface RMS (waves) A)Input	B)Inpt-BFP	C)Correctd	Correctability (%) (A-B)/A	(A-C)/A	(B-C)/B
1	2.1444E-02	8.2222E-03	**5.9258E-03**	61.657	72.366	**27.929**

Force Actuators

Load	Surface RMS (waves) A)Input	B)Inpt-BFP	C)Correctd	Correctability (%) (A-B)/A	(A-C)/A	(B-C)/B
1	5.1001E-01	2.2387E-01	**5.9258E-03**	56.105	98.838	**97.353**

The force actuators have a higher percent correctability due to the high initial deformation under 1g on 3 points. However, the corrected RMS is the same for both force and displacement actuators.

3.2 Surface Correction

Actuators are used to minimize the RMS surface error /deviation from a desired surface:

E = error = $\Sigma\, w_i\, (di_i + da_i)^2$
w_i = area weighting of node i = fraction of total area
di_i = input displacement at node i = unwanted disturbance
da_i = actuated displacement at node i = $\Sigma\, x_j\, dx_{ji}$
x_j = actuator j input (force or displacement)
dx_{ji} = displacement at node i due to unit input at actuator j

Find X (the vector of all x_i) which minimizes E by $dE/dX = 0$. This results in a linear system:

$H\,X = F$ where $H_{jk} = \Sigma\, w_i\, dx_{ji}\, dx_{ki}$ and $F_k = \Sigma\, w_i\, di_i\, dx_{ki}$

From the solution of X, the actuated surface da is obtained, and subsequently the corrected surface dc.

dc_i = corrected displacement at node i = $di_i + da_i$

The mathematical procedure is similar to fitting Zernike polynomials[1].

The following surface correctability terms can be defined:

R_i = RMS of (input surface)
R_b = RMS of (input surface - BFP)
R_f = RMS of (input surface - BFP - Power)
R_c = RMS of (corrected surface = input surface + actuated surface)

C_b = Correctability due to Perfect Rigid Body Compensation = $(R_i - R_b) / R_i$
C_f = Correctability due to Perfect Focus Compensation = $(R_b - R_f) / R_b$

C_{ab} = Actuator Correctability after Perfect Rigid Body Compensation = $(R_b - R_c) / R_b$
C_{af} = Actuator Correctability after Perfect Focus Compensation = $(R_f - R_c) / R_f$
C_{at} = Total Actuator Correctability = $(R_i - R_c) / R_i$

The total actuator correctability (C_{at}) can be misleading and overstate the effectiveness of deformable optics. The true effect of deforming (not pointing or focusing) is C_{af}. If there are no external pointing or focusing mechanisms, then the actuators are the only effect, so total actuator correctability is significant. In this last condition, the actuator set should include rigid body motion capability.

3.3 Example

An adaptive, segmented primary mirror with 6 petals on a mount structure was subjected to a 1g lateral load and 55C uniform temperature increase. Each segment has 3 displacement actuators for rigid motion control and 19 force actuators for surface deformation control. The correctability was determined for rigid body motion correction and for surface deformation correction. Figures 7-A through 7-D show the deformed surface. Figure 7-E shows rigid body motion correction of 3 displacement actuators/segment, Figure 7-F shows the effect of the 19 force actuators on surface deformation control.

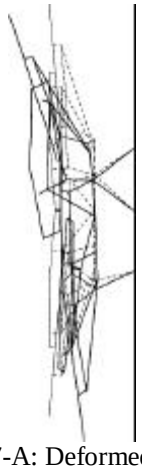

Figure 7-A: Deformed side view

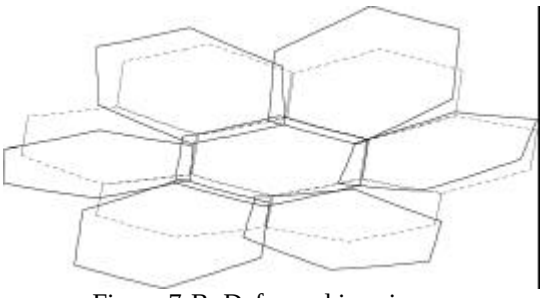

Figure 7-B: Deformed iso view

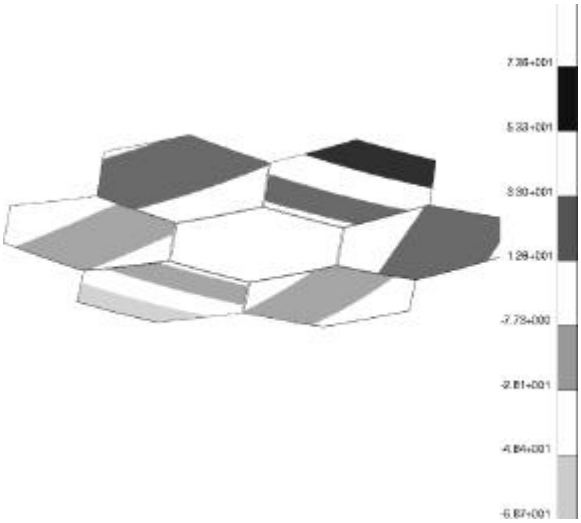

Figure 7-C: Input displacement (RMS=28.0)

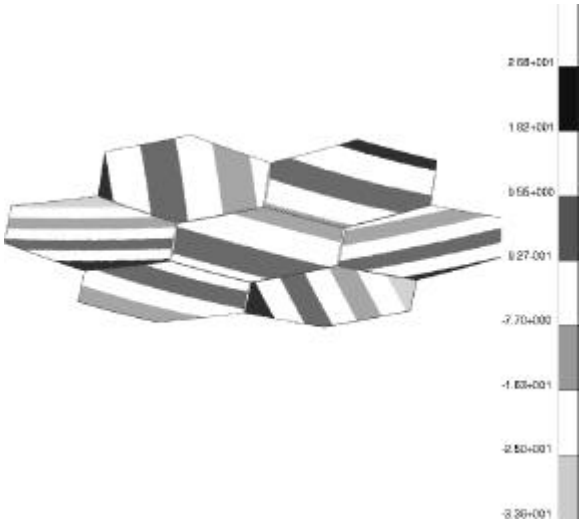

Figure 7-D: Best-Fit plane removed (RMS=11.1)

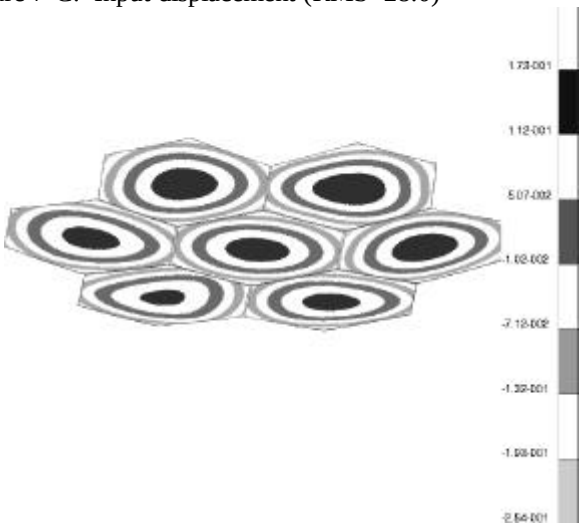

Figure 7-E: With Segment Rigid Body Motion Correction (RMS=0.09)

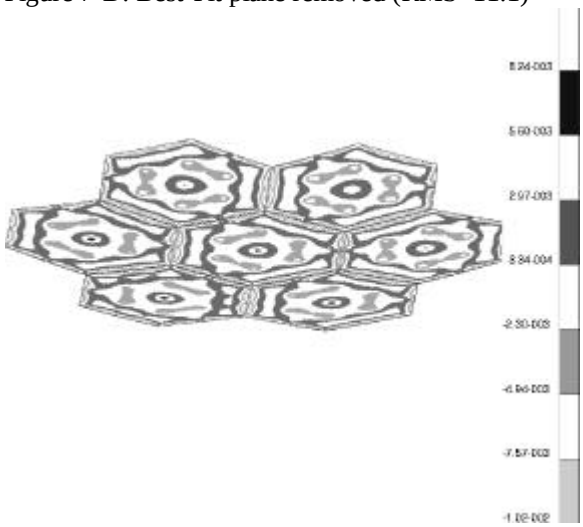

Figure 7-F: With Surface Correction (RMS=0.003)

3.4 Practical Analysis Issues

From a programmer's and/or analyst's viewpoint, there are several practical considerations. The displacement vector size depends on the number of nodes on the optical surface. This effects the number of "rows" in each input surface and each actuator influence function. The number of columns is affected by the number of load cases for the input surface and the number of actuators for the influence matrix. Thus, array size and solution times can be an issue for highly detailed models with a large number of actuators.

Symmetry can be used effectively to reduce matrix sizes. In most applications, the optic and actuator arrangement have at least 1 plane of symmetry. If the input surface (load case) also has the same symmetry, then a symmetric model is obvious efficiency improvement. With a little programming effort or proper tools, full surface plots are quite easy to obtain from symmetric sub-models.

For segmented optics, there may be no cross-talk in the actuator influence functions from segment to segment. If that is the case, then reduced vector sizes are possible. Also, if the segments are identical, then the influence functions are identical from segment to segment and can all be obtained from running a single segment. Some programming effort is required to take advantage of these data reduction features.

In practice, the deformable mirror's performance is determined by the number and placement of sensors. In the equations above, the area weighting vector was applied to all of the nodes on the surface. In which case, the predicted actuator inputs are those which minimize the full surface RMS. If however, only a subset of nodes are sampled by sensors which drive the actuators, then the actuator inputs will be those which minimize the RMS over the sampled points. This can be predicted mathematically by using an area weighting which is non-zero only at the sensor locations. In SigFit, this is accomplished through a user defined area weighting vector.

A similar effect occurs in the case when pointing/focus are determined by the center segment (possibly a stiff mirror without actuators) only. The deformable petals are then driven to match the stiff center. Again, this feature can be handled through the use of a separate weighting functions for best-fit-plane and focus (center segment only) from the corrected surface weighting function (all segments). In SigFit, this is easily input via property numbers of the various segments.

4.0 DYNAMIC PERFORMANCE

4.1 Analysis Issues

In the dynamic response of a segmented optic, the analyst may be interested in various measures of the surface motion. For example,

1) the full surface average pointing error
2) the full surface RMS error (best-fit-plane removed)
3) individual segment pointing error

Each of these may have an individual line item error budget, and they may each have a separate method of reducing the response through improved design or adaptive/active control. To obtain these responses, special modeling techniques and tools are required.

4.2 Frequency Response

Frequency response analysis is the prediction of structural behavior to a steady-state harmonic input. A common solution approach for large problems is to use the modal method[4]. In this technique, we first solve for undamped natural frequencies from,

$$\left(-w_j^2[M]+[K]\right)\Phi_j = 0 \quad , \qquad 4.2\ (1)$$

where, Φj is the eigenvector for the jth mode, ω_j^2 is the eigenvalue, $(2\ \pi\ f_j)^2$, for the jth mode, M is the mass matrix, and K is the stiffness matrix. The modal approach creates uncoupled equations of motion by the substitution,

$$U = \sum z_i \Phi_j \quad , \qquad 4.2\ (2)$$

where, z_j is the modal coordinate representing the response of mode j. Any physical response such as displacement or stress is then the scaled combination of such responses from the modal analysis. Equation 4.2 (2) would be used to recover displacements and stresses would be recovered with,

$$s = \sum z_i S_j \qquad 4.2\ (3)$$

where, S_j is the modal stress for the jth mode.

For optical performance calculation, efficiencies can be realized using the modal approach. If each mode j be decomposed into,

T_j = pointing vector (R-B or BFP) for the jth mode
P_j = power for the jth mode
V_j = the residual vector for the jth mode = Φ_j -BFP - power

then, the net surface pointing error and the net surface power are obtained from,

$$T_n = \sum z_j T_j \qquad P_n = \sum z_j P_j \qquad \text{4.2 (4a ,4b)}$$

and the net surface RMS is obtained from the combined residual vectors,

$$RMS_n = RMS\left(\sum z_j V_j\right). \qquad \text{4.2 (5)}$$

In all of these calculations, care must be taken because z is a complex quantity. For typical sine sweep analyses with many frequency steps and relatively few modes, the modal approach using these decompositions is more efficient than direct solution techniques.

For individual segment pointing error, a modeling trick may be used. An interpolation element (RBE3) should be constructed connecting all nodes on the optical surface with an average surface point for each individual segment. A rigid link connects each average surface point to its own individual focus point located at the center of curvature or focal point. Under dynamic distortion the motions of the individual focus points can be processed to measure the mismatch of segment pointing or "blur" (Fig 8). Again, this can be made more efficient using the modal approach.

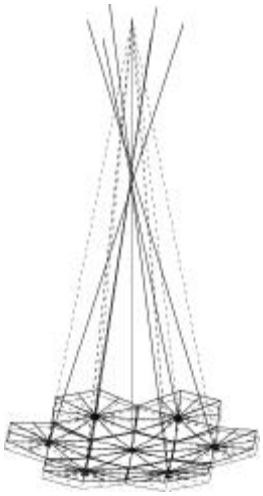

Figure 8: Segment pointing

4.3 Random Response

The sine sweep response from a frequency response analysis is called a transfer function, or frequency response function, FRF, and is the forcing frequency dependent magnitude of the complex response. In random response, the statistical nature of the load is given as a load power spectral density, PSD_P. The statistical nature of output is found as a response power spectral density, PSD_R, from the equation,

$$PSD_R = FRF^2 PSD_p \qquad \text{4.3 (1)}$$

The temporal RMS of the response is given as,

$$RMS_R = \sqrt{A} \qquad \text{4.3 (2)}$$

where, A is the area under the PSD_R curve.

Common response levels used in performance predictions are as follows:

1σ = 1 x RMS value => response is less than 1σ for 68.3% of the time
3σ = 3 x RMS value => response is less than 3σ for 99.7% of the time

For image motion or average surface pointing under random loading:

1) Include a multipoint constraint (MPC) for image motion or BFP in model
2) Run random analysis in FE program, output 1σ of image motion/BFP

or

1) Calculate natural frequencies and mode shapes Φ
2) Use modal techniques to find each optic motion at each frequency step
3) At each frequency step, calculate image motion response (FRF)
4) At each frequency step, calculate PSD_R of image motion
5) Find the square-root of the area under the PSD_R response curve to get the 1σ value

In the calculation of the 1σ value of surface RMS, all sign and phasing information has been lost due to the use of the FRF, which is the magnitude of the frequency dependent complex response. Therefore, it is <u>not</u> correct to find 1σ motion of each optic then combine to find image motion.

For optical surface RMS under random loading:

1) Calculate natural frequencies and mode shapes Φ
2) Calculate and subtract rigid-body motions if desired
3) Use modal techniques to find surface displacements at each frequency step
4) At each frequency step, calculate surface RMS response (FRF)
5) At each frequency step, calculate PSD_R of surface RMS
6) Integrate under PSD_R response and square-root, to get 1σ value of surface RMS

As was the case with the image motion calculation, the 1σ values have lost all sign and phasing information, so it is not correct to find 1σ of each node then combine to find surface RMS.

If this calculation is also performed for each mode individually, each mode's fractional contribution to the total pointing and surface RMS random response is determined. This allows the analyst to identify problem mode shapes which should be considered during improvement of the design.

When the mounted, segmented mirror discussed above is given a random vertical (Z) base shake with a PSD input shown (Fig 9-A), then the surface RMS has a 1-sigma random response of 0.67 microns (Fig 9-B).

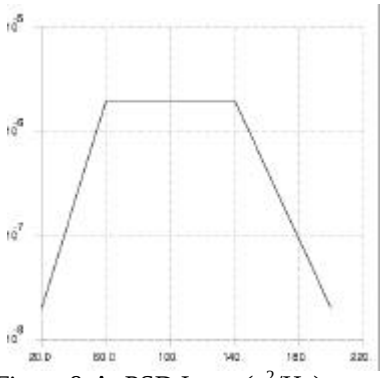

Figure 9-A PSD Input (g^2/Hz)

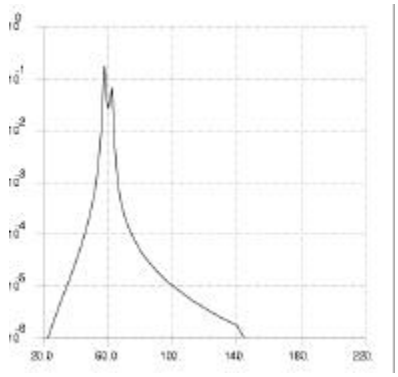

Fig 9-B PSD Surface RMS Z shake

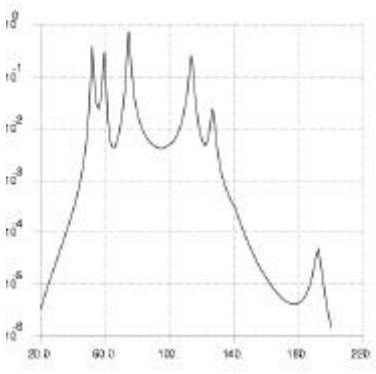

Fig 9-C PSD Surface RMS Y shake

The random response analysis was conducted in SigFit using modal methods. The printed output from SigFit in Table 3 shows that 70% of the response was due to Mode 6 and 30% due to Mode 9. Figures 10-A and 10-B show deformed plots of these modes.

Table 3: Modal Contributions to Surface RMS random response due to vertical (Z) base shake

Each modes % contribution to PSD for Surface= 1

Mode	Freq	RB-Tx	RB-Ty	RB-Tz	RB-Rx	RB-Ry	d-Pow	d-Bia	**S-RMS**	R-RMS
4	51.73	13.579	0.000	0.000	0.000	31.525	0.000	0.000	0.000	0.000
5	51.74	2.480	.473	0.000	4.284	5.887	0.000	0.000	0.000	0.000
6	57.88	27.688	.105	99.996	61.036	5.884	99.996	99.996	**69.772**	99.996
7	59.46	16.025	0.000	0.000	0.000	31.521	0.000	0.000	0.000	0.000
8	59.46	11.307	2.323	0.000	17.860	22.944	0.000	0.000	.001	0.000
9	62.42	.220	6.475	.004	1.340	1.146	.004	.004	**30.225**	.004
10	72.00	.032	0.000	0.000	0.000	.011	0.000	0.000	0.000	0.000
11	74.45	.797	0.000	0.000	0.000	.038	0.000	0.000	0.000	0.000
12	74.46	14.459	42.780	0.000	6.505	.335	0.000	0.000	.001	0.000
13	74.46	1.606	0.000	0.000	0.000	.064	0.000	0.000	0.000	0.000
14	74.63	.598	39.659	0.000	8.931	.005	0.000	0.000	.001	0.000
15	74.63	10.889	0.000	0.000	0.000	.639	0.000	0.000	0.000	0.000
16	109.22	.003	0.000	0.000	0.000	0.000	0.000	0.000	0.000	0.000
17	113.17	.022	2.656	0.000	.037	0.000	0.000	0.000	0.000	0.000
18	113.18	.122	0.000	0.000	0.000	0.000	0.000	0.000	0.000	0.000

..... truncated

For a horizontal base shake (Y direction) of the same magnitude, the surface had a 1-sigma response of 2.0 microns (Fig 9-C). Several modes had a significant contribution as shown in the printed output from SigFit in Table 4.

Table 4: Modal Contributions to Surface RMS random response due to horizontal (Y) base shake

Each modes % contribution to PSD for Surface= 1

Mode	Freq	RB-Tx	RB-Ty	RB-Tz	RB-Rx	RB-Ry	d-Pow	d-Bia	**S-RMS**	R-RMS
4	51.73	48.771	0.000	0.000	0.000	49.239	0.000	0.000	0.000	0.000
5	51.74	48.135	15.758	.820	96.622	49.691	12.424	12.425	**17.788**	9.441
6	57.88	0.000	0.000	1.516	0.000	0.000	4.106	4.106	0.000	0.000
7	59.46	.612	0.000	0.000	0.000	.523	0.000	0.000	0.000	0.000
8	59.46	.595	.210	6.566	1.093	.525	8.222	8.223	**13.670**	.230
9	62.42	0.000	0.000	4.624	0.000	0.000	12.843	12.844	0.000	0.000
10	72.00	0.000	0.000	0.000	0.000	0.000	0.000	0.000	0.000	0.000
11	74.45	0.000	0.000	0.000	0.000	0.000	0.000	0.000	0.000	0.000
12	74.46	.453	2.298	42.194	.237	.005	29.841	29.840	**15.974**	3.507
13	74.46	.566	0.000	0.000	0.000	.010	0.000	0.000	0.000	0.000
14	74.63	.078	8.832	34.942	1.347	0.000	30.921	30.920	**28.378**	15.761
15	74.63	.111	0.000	0.000	0.000	.003	0.000	0.000	0.000	0.000
16	109.22	0.000	0.000	0.000	0.000	0.000	0.000	0.000	0.000	0.000
17	113.17	.341	71.573	3.126	.668	.003	.191	.191	**22.041**	69.638
18	113.18	.333	0.000	0.000	0.000	.001	0.000	0.000	0.000	0.000

..... truncated

4.4 Transient Response

Transient response is determined by solving by numerical integration the dynamics equation,

$$[M]\{\ddot{U}\}+[B]\{\dot{U}\}+[K]\{U\}=\{P(t)\}. \qquad 4.4\ (1)$$

Either the direct method or modal method may be used. As with frequency response, the modal method is more efficient on many problems. As in the modal method for frequency response, the pointing, focus and residual terms can be determined for each mode shape and added using modal addition. In a transient response, the user may want curves of response over the time range of interest, or more often, just the peak values. In SigFit, every peak response is identified along with it's time of occurrence.

5.0 SUMMARY

Standard finite element results are usually not in a convenient form for opto-mechanical analysis. The output must be post-processed to decompose the displacements into rigid-body motion, power, and higher order aberrations. In the presence of radial motion, the finite element displacements must be used to compute scalar surface deviation before optical quantities are calculated. Segmented optics present unique post-processing challenges, since it is often useful to determine assembly pointing and wavefront error as well as individual segment pointing and wavefront errors. With adaptive optics, the interest is in understanding and maximizing the correctability of the system. The dynamic analysis of optics usually requires similar decomposition into rigid body motion and wavefront error, but requires efficient algorithms to handle the many analysis steps. Typically, specialized post-processing software is required.

6.0 REFERENCES

1) V. Genberg, "Optical Surface Evaluation", SPIE Proc. Vol. 450, Paper 450-08, Nov 1983.
2) M. Born & E. Wolf, *Principles of Optics*, Pergamon Press, New York, 1964.
3) SigFit Documentation, Sigmadyne, Inc., Rochester, NY, 2001.
4) R. Craig, *Structural Dynamics*, John Wiley & Sons, New York, 1981.